ORGANOMETALLICS

Article

pubs.acs.org/Organometallics

[FeFe]-Hydrogenase Synthetic Mimics Based on *Peri*-Substituted Dichalcogenides

Carlotta Figliola,[†] Louise Male,[†] Peter N. Horton,[‡] Mateusz B. Pitak,[‡] Simon J. Coles,[‡] Sarah L. Horswell,*[,†] and Richard S. Grainger*[,†]

[†]School of Chemistry, University of Birmingham, Edgbaston, Birmingham B15 2TT, U.K.

[‡]UK National Crystallography Service, Chemistry, Faculty of Natural and Environmental Sciences, University of Southampton, Southampton, SO17 1BJ, U.K.

Supporting Information

ABSTRACT: Eight dithiolato-, diselenolato-, and mixed S,Se-$Fe_2(CO)_6$ complexes based on *peri*-substituted naphthalene and phenanthrene dichalcogenides are prepared by oxidative insertion of $Fe_3(CO)_{12}$ into the dichalcogen bonds of 2,7-dimethoxynaphtho[1,8-*cd*][1,2]dithiole, three naphtho[1,8-*cd*][1,2]diselenoles, two naphtho[1,8-*cd*][1,2]-thiaselenoles, phenanthro[1,10-*cd*][1,2]dithiole, and phenanthro[1,10-*cd*][1,2]diselenole. Complexes are characterized by ^{1}H, ^{13}C NMR, UV/vis, and IR spectroscopy and by X-ray analysis. The effect of replacing sulfur with selenium, incorporating electron-donating groups (2,7-di-*tert*-butyl, 2,7-dimethoxy) on the naphthalene ring system, and changing the degree of conjugation in the aromatic backbone (naphthalene vs phenanthrene) on the reduction potential is evaluated by cyclic voltammetry. The electrocatalytic activity of these [FeFe]-hydrogenase synthetic mimics for proton reduction in the presence of increasing concentrations of *p*-TsOH is investigated. Diselenolate-based [FeFe]-complexes show enhanced catalytic activity for proton reduction compared with their sulfur congeners.

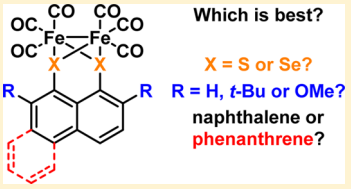

INTRODUCTION

The enzyme [FeFe]-hydrogenase catalyzes proton reduction and, therefore, the production of molecular hydrogen at high turnover rates (TOF in the order of 9000 s^{-1}).[1] $Fe_2(CO)_6$ clusters bound to bridging dithiolate ligands have been the subject of intense interest as synthetic models for the active site of [FeFe]-hydrogenase.[2] Variation in the dithiolate ligand backbone and systematic replacement of the carbonyl ligands have been investigated in efforts directed at both better understanding of the biological system and in the search for synthetic catalysts which can reduce protons to molecular hydrogen at reduced overpotentials and increased rates.[3]

In 2009, Tilley investigated [FeFe]-complexes **1a**−**c** incorporating naphthalene-1,8-dithiolate ligands as models of the enzymatic active site (Figure 1).[4] The three-atom linker between the two sulfur atoms mimics that found in the natural system, and the rigidity of the naphthalene ring stabilized the reduced form of the complex compared with saturated dithiolate ligand-based complexes. Substituents on the naphthalene ring were found to modify the reduction potentials of the complexes and, to a lesser extent, the rate of electrocatalytic proton reduction. On the basis of these findings, more elaborate naphthalene dithiolate based synthetic mimics of [FeFe]-hydrogenase have been prepared.[5,6] The rigid phenanthrene-based system **2** was subsequently reported to be reduced at less negative potentials than **1a**−**c**, which was ascribed to the greater electron-withdrawing and delocalization properties of the aromatic π-system.[7]

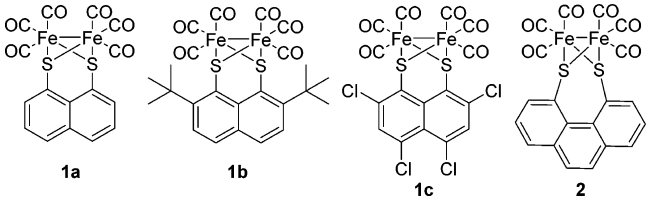

Figure 1. Synthetic mimics of [FeFe]-hydrogenase based on naphthalene-1,8-dithiolate and phenanthrene-4,5-dithiolate ligands.[4−7]

Another strategy to increase the catalytic activity of [FeFe]-hydrogenase model systems toward proton reduction is to replace the two sulfur atoms with heavier chalcogens.[8−20] The first examples of diselenolate-based [FeFe]-complexes investigated as synthetic mimics of the enzyme active site were published in 2008 by Peng and co-workers.[9] The *N*-substituted azapropanediselenolate-bridged [FeFe]-complexes **3a**−**c** showed the same reduction potentials but enhanced reactivity as proton reduction catalysts compared with the corresponding azapropanedithiolates (Figure 2). In the same year, Weigand reported the synthesis and characterization of sugar-based diselenolate [FeFe]-complex **4**, which in comparison with the corresponding dithiolate-based complex, was more reactive toward molecular hydrogen production, despite being reduced at more negative potential.[10] In addition, the selenium-based complex showed higher stability over the sulfur analogue upon deacetylation in an approach toward water-soluble catalysts. In 2009, Song reported the synthesis and characterization of the

Received: June 28, 2014
Published: August 18, 2014

   dx.doi.org/10.1021/om500683p | *Organometallics* 2014, 33, 4449−4460

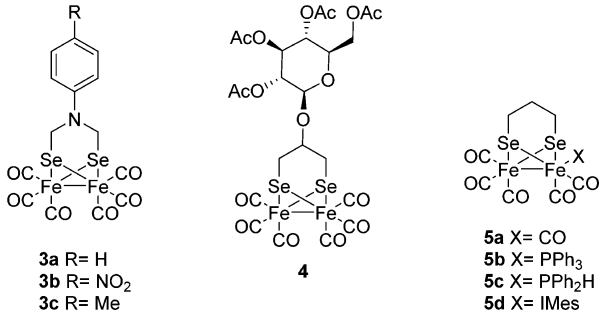

Figure 2. Representative synthetic mimics of [FeFe]-hydrogenase based on diselenolate ligands.[9−11]

propanediselenolate-based [FeFe]-complexes **5a−d**, which again showed better electrocatalytic activity for proton reduction than the corresponding propanedithiolate-based [FeFe]-complexes.[11] Further studies confirmed the general trend that selenium-based systems are often more active catalysts for proton reduction despite being reduced at more negative potentials than their sulfur equivalents.[8]

As part of our ongoing interest in the chemistry of *peri*-substituted dichalcogenides,[21−25] we herein report the synthesis, characterization, and study of new synthetic mimics of the [FeFe]-hydrogenase active site.[26] First, we have expanded the range of naphthalene-1,8-dithiolato-$Fe_2(CO)_6$ complexes, synthesizing **1d** with two electron-donating groups (OMe) in positions 2 and 7 on the naphthalene ring (Figure 3). Second,

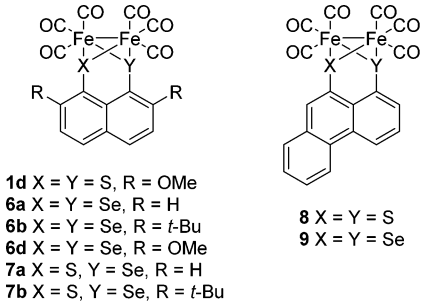

Figure 3. [FeFe]-hydrogenase synthetic mimics based on *peri*-substituted dichalcogenides prepared in this study.

to study the effect of the chalcogen on the catalytic properties, we have prepared [FeFe]-complexes based on naphthalene-1,8-diselenolates **6a**, **6b**, and **6d** and naphthalene-1,8-thioselenolates **7a** and **7b**. In addition, to investigate further the impact of the ligand backbone on the stability of the reduced species, we have synthesized [FeFe]-complexes based on phenanthrene-1,8-dithiolate, **8**, and the corresponding diselenolate, **9**. The [FeFe]-complexes show reduction potentials comparable with the values for known synthetic mimics **1a−c**,[4] with the diselenolate-based complexes **6a**,**b**,**d** and **9** displaying enhanced catalytic activity for proton reduction compared with the equivalent dithiolate complexes.

RESULTS AND DISCUSSION

Synthesis and Characterization. The dichalcogenide ligands and the corresponding [FeFe]-complexes were synthesized as shown in Scheme 1. Known dichalcogens **10d**,[23] **11a**,[27,28] **11b**,[29] **11d**,[29] **12a**,[30−32] and **13**[33] were prepared according to literature procedures, with the exception of 2,7-di-*tert*-butylnaphtho[1,8-*cd*][1,2]diselenole (**11b**), where $FeCl_3$

Scheme 1. Synthesis of Dichalcogens and Corresponding [FeFe]-Complexes

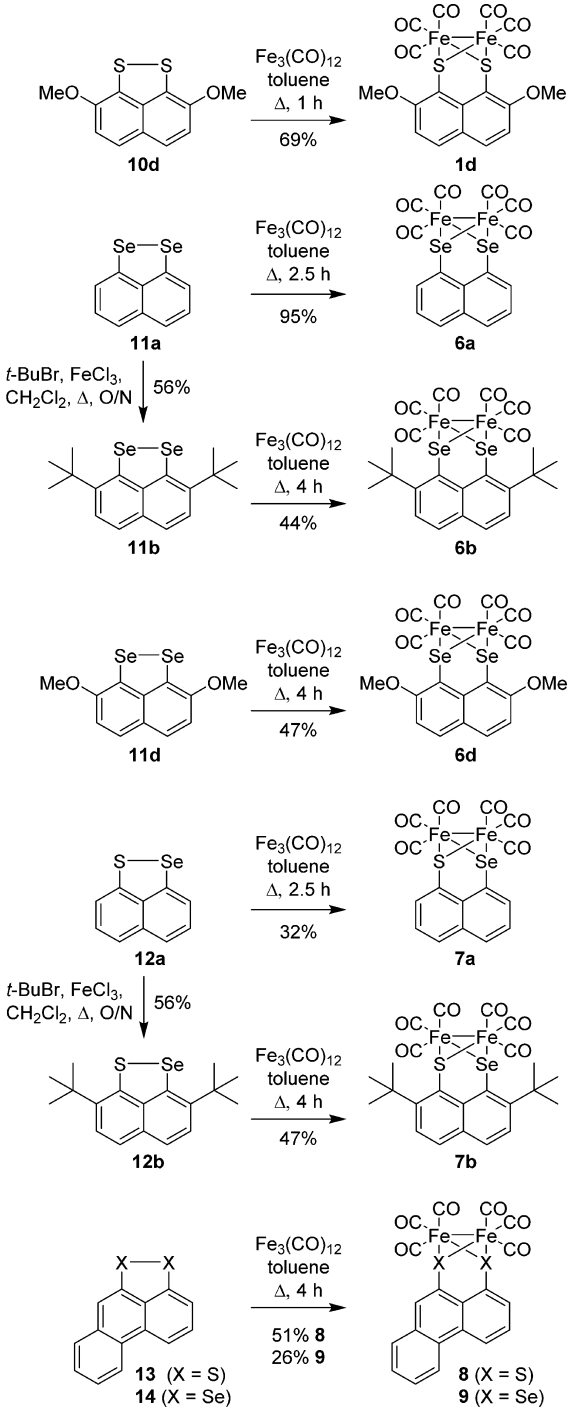

was used in preference to $AlCl_3$ as Lewis acid for the regioselective Friedel−Crafts reaction of compound **11a**.[23] The novel dialkylated mixed dichalcogen **12b** was similarly prepared from **12a**. The synthesis of phenanthrene disulfide **13** from 9-bromophenanthrene[33] was modified to prepare the novel phenanthro[1,10-*cd*][1,2]diselenole (**14**) by substituting selenium for sulfur in the quench of 1,10-dilithiophenanthrene.

[FeFe]-complexes **1d**, **6a**,**b**,**d**, **7a**,**b**, **8**, and **9** were obtained in variable yields by simply refluxing the corresponding dichalcogens **10d**, **11a**,**b**,**d**, **12a**,**b**, **13**, and **14** with $Fe_3(CO)_{12}$ in toluene (Scheme 1). In contrast to the original report by

dx.doi.org/10.1021/om500683p | *Organometallics* 2014, 33, 4449−4460

Tilley on the synthesis of **1a**–**c**,[4] but consistent with later reports for related *peri*-substituted naphthalene disulfides,[6,7] the [FeFe]-complexes could be prepared directly through oxidative insertion into the dichalcogen bond without the need to first reduce to the potentially readily oxidized dithiol, thiaselenol or diselenol.

We also attempted to prepare complex **6c**, the selenium analogue of dithiolato-complex **1c**. Although 3,5,6,8-tetrachloronaphtho[1,8-*cd*][1,2]diselenole (**11c**) was successfully synthesized from **11a** by adapting the reported procedure for the corresponding tetrachlorodithiole,[4] complex **6c** could not be obtained from **11c** by heating with $Fe_3(CO)_{12}$ in toluene (Scheme 2). Compound **11c** degrades in refluxing toluene, and its poor solubility does not promote oxidative insertion at room temperature.

Scheme 2. Attempted Preparation of 6c

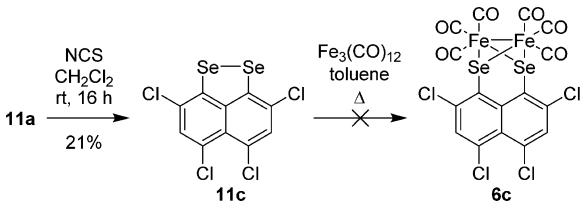

The novel [FeFe]-complexes **1d**, **6a**,**b**,**d**, **7a**,**b**, **8**, and **9** were characterized by ^{1}H and ^{13}C NMR, UV/vis and IR spectroscopy and by X-ray crystallography. ^{1}H NMR showed the expected aromatic signals which are shifted downfield compared with the corresponding dithiole, diselenole or thiaselenole precursor. As for compounds **1a**–**c**,[4] the ^{13}C NMR of the [FeFe]-complexes contain a characteristic peak at 207–209 ppm, assigned to the carbonyl ligands.

IR spectroscopy confirmed the insertion of the $Fe_2(CO)_6$ into the dichalcogen bond. Infrared stretching vibrations of the carbonyl groups in the [FeFe]-complexes are affected by the nature of the chalcogen (sulfur or selenium), the naphthalene substituents (*t*-Bu or OMe) and the aromatic backbone (naphthalene or phenanthrene). The wavenumber values for the carbonyl infrared stretching vibrations for **1d**, **6a**,**b**,**d**, **7a**,**b**, **8**, and **9** (Table 1) are in line with previously reported synthetic mimics which showed the wavenumbers for the carbonyl ligands bonded to the two iron centers in the region 2070–1800 cm^{-1}.[3,4]

The CO stretching vibrations for selenium compounds are generally shifted to lower wavenumbers compared with the sulfur systems, with the mixed S,Se-complexes showing intermediate values (compare complexes **1a**, **6a** and **7a**, **1b**, **6b** and **7b**, and **1d** and **6d**, Table 1). Selenium is less electronegative than sulfur; hence, the electron-densities at the iron centers are higher when coordinated to the selenium-based ligands thus favoring π-backbonding from the iron centers to the carbonyl ligands and shifting the carbonyl stretching toward lower wavenumber. Similar trends have previously been observed in comparing chalcogens in [FeFe]-hydrogenase mimics.[8] The phenanthrene-based systems **8** (S,S) and **9** (Se,Se) mirror this trend for the highest two wavenumbers, but not for the lower four wavenumbers, which are higher for selenium than for sulfur.

Table 1. Carbonyl Infrared Stretching Vibrations for [FeFe]-Complexes 1d, 6a,b,d, 7a,b, 8, and 9

complex	ν(CO) (cm^{-1})
1a[a]	2074, 2039, 2001
1b[a]	2071, 2036, 1997
1d	2061, 2021, 1976, 1955, 1878
6a	2058, 2016, 1996, 1979, 1822
6b	2057, 2015, 1979, 1970, 1956
6d	2054, 2014, 1970, 1950, 1875
7a	2061, 2020, 1999, 1982, 1958, 1822
7b	2061, 2017, 1980, 1972, 1961, 1940
8	2065, 2028, 1978, 1957, 1946, 1936
9	2055, 2021, 1996, 1976, 1962, 1942

[a]Data taken from ref 4.

Tilley has previously noted that the electron-donating *tert*-butyl substituents on **1b** cause a bathochromic shift in the IR carbonyl stretching frequencies compared with **1a**.[4] The infrared stretches shift toward even lower wavenumbers for the methoxy-substituted naphthalene **1d**, suggesting a stronger electron-donating effect than the *tert*-butyl groups exert in **1b**. The same trend is observed for diselenolate-based [FeFe]-complexes **6a**, **6b**, and **6d**, with the exception of the lowest wavenumber, where the opposite trend is seen (Table 1).

A comparison of naphthalene dithiolate **1a** with phenanthrene-based dithiolate **8** shows the additional conjugation in the phenanthrene ring causes a bathochromic shift in the IR stretching vibrations of the carbonyl groups in the sulfur series. The effect in the selenium series is less clear-cut, with corresponding vibrations for diselenolate **6a** and phenenathrene diselenolate **9** shifting to both higher and lower wavenumbers.

The UV/vis spectra of the [FeFe]-complexes are shown in Figure S1 (Supporting Information), and the corresponding values for the extinction coefficient are reported in Table S1 (Supporting Information). The optical spectra show the expected intense absorption band in the range 300 and 360 nm (ε = 10^3–10^4 M^{-1} cm^{-1}), attributed either to a $\pi \rightarrow \pi^*$ transition from the aromatic backbone or to a charge transfer from the iron centers to the carbonyl ligands.[34,35] The UV/vis spectra of the dichalcogen precursors were also recorded in acetonitrile (Figure S1, Supporting Information). The dichalcogens display similar absorption bands but of lower energies and broadened shapes.[6] For complexes **1d**, **6b**, and **6d**, it is possible to discern a shoulder between 380 and 420 nm (ε = 10^1–10^2 M^{-1} cm^{-1}), which is consistent with a d–d transition.[7,34]

X-ray Crystallography. The molecular structures of [FeFe]-complexes **1d**, **6a**,**b**,**d**, **7a**,**b**, **8**, and **9** were confirmed by X-ray analysis. In the case of **6d** the structure, called **6d_DCM**, includes a molecule of dichloromethane solvent, with a polymorph not including the solvent given in the Supporting Information. Crystal structures are shown in Figure S2 (Supporting Information) (**6a** and **7a**), Figure 4 (**6b** and **7b**) Figure S3 (Supporting Information) (**1d** and **6d_DCM**), Figure S4 (Supporting Information) (**8**), and Figure 5 (**9**), bond lengths and angles are listed in Table 2, and crystal data and structure refinement details are described in Table S2 (Supporting Information). As a result of problems with the crystal, and thus data quality, the structure determination of **1d** is less reliable than the others, and consequently, in the following comments only broad comparisons involving structural parameters from this species are made.

All of the crystal structures possess a dichalcogenide-bridged [FeFe]-core which assumes the typical butterfly architecture and in which the two iron centers are linked to three carbonyl

dx.doi.org/10.1021/om500683p | *Organometallics* 2014, 33, 4449–4460

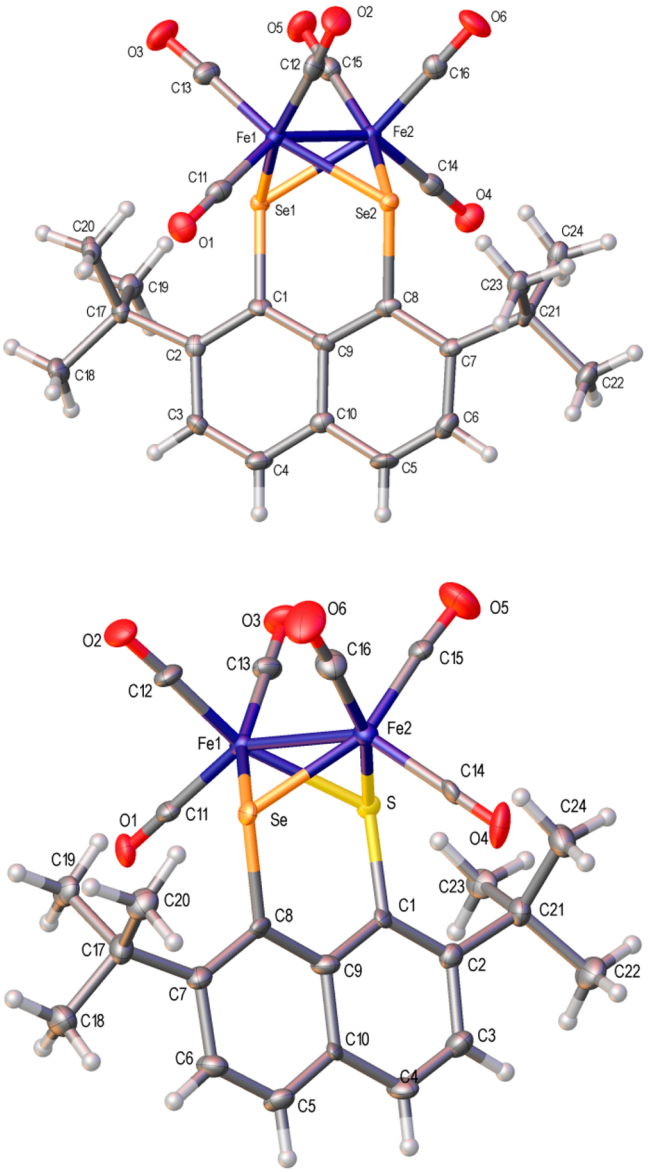

Figure 4. Crystal structure of complex **6b** (top) and **7b** (bottom) with ellipsoids drawn at the 50% probability level. In **7b** the structure contains two crystallographically independent molecules, of which only one is shown and the sulfur and selenium atoms are both disordered over two positions with the minor component having been omitted for clarity.

ligands in a distorted square-pyramidal geometry, as previously reported for **1a** and **1c**.[4] The Fe−Fe bond length for each complex is comparable with those reported in the literature for the active site of [FeFe]-hydrogenase (2.6 Å), as well as the bond length between each iron and each chalcogen (Fe1−S1 = Fe1−S2 = Fe2−S2 = Fe2−S2 = 2.3 Å in the enzyme).[2] The phenanthrene-1,10-dithiolate-based [FeFe]-complex **8** has comparable bond lengths and angles with the data reported for the literature compound **1a** in Table 2,[4] which shows that the extra aromatic ring has minimal effect on the general structure. Similarly, the parameters in **6a** and **9** are comparable. The iron−chalcogen bond lengths are longer for selenium than sulfur (compare **1a**, **6a** and **7a**, **1d** and **6d_DCM**, and **8** and **9** in Table 2) as expected on electronegativity grounds.[9]

Electron-donating groups (*t*-Bu, OMe) on the naphthalene ring have little effect on the Fe−X bond length. However, the

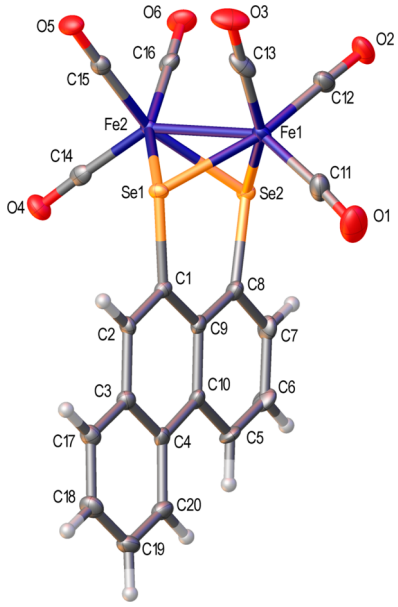

Figure 5. Crystal structure of complex **9** with ellipsoids drawn at the 50% probability level. The structure contains two crystallographically independent molecules, of which only one is shown.

two bulky *tert*-butyl groups in the *ortho* positions on the ring decrease the nonbonding distance between the chalcogen atoms (as seen in the observed values of Se1···Se2 distances for **6a**, **6b**, and **6d_DCM** (3.1939(6), 3.1374(9), and 3.2101(12) Å respectively, Table 2). The van der Waals repulsion of the *tert*-butyl groups also cause a displacement of the chalcogens either side of the naphthalene plane, as seen in the X−C(1)···C(8)−Y torsion angle (Table 2).[22,23,29,36] This effect is more pronounced for **6b** than **7b** because of the relative size of selenium and sulfur. A third pronounced effect of the *tert*-butyl groups is on the alignment of the Fe−Fe bond with the plane of the naphthalene ring. For all of the complexes except **6b** and **7b**, the Fe−Fe bond is aligned nearly perpendicular to the plane of the aromatic ring system (see Table 2, angles between planes 1 and 2). In comparison, the 2,7-di-*tert*-butyl naphthalene systems **6b** and **7b** are notably twisted by 20 °C (see projections in Figure 6), slightly more for **6b** (68.91(9)°), containing two selenium atoms, than **7b** (71.4(2)°), containing one selenium and one sulfur. The disruption of symmetry in **6b** could help explain its anomalous electrochemical behavior (vide infra).

Electrochemical Characterization. Cyclic voltammetry (CV) was employed to investigate the electrochemical properties of complexes **1d**, **6a**,**b**,**d**, **7a**,**b**, **8**, and **9**. Measurements were recorded with ferrocene as an internal reference and all potentials herein are quoted with respect to Fc^+/Fc. Figures 7 and 8 show the CVs recorded for these complexes. Each complex gives two reduction waves, which are assigned to $Fe^IFe^I \rightarrow Fe^IFe^0$ and $Fe^IFe^0 \rightarrow Fe^0Fe^0$, and one/two oxidation events, which are assigned to $Fe^IFe^I \rightarrow Fe^IFe^{II}$ and $Fe^IFe^{II} \rightarrow Fe^{II}Fe^{II}$, by analogy with data previously reported for similar complexes.[4] The half-wave potentials, $E_{1/2}$, derived from the CVs are all reported in Table 3, along with literature values for complexes **1a** and **1b**.[4]

The peak separations of the first reduction waves are all greater than that observed for the Fc^+/Fc internal redox couple, indicating quasi-reversible behavior (intermediate electron transfer kinetics) in each case. The second reduction wave

dx.doi.org/10.1021/om500683p | *Organometallics* 2014, 33, 4449−4460

Table 2. Selected Bond Lengths (Å) and Angles (deg) for Compounds 1a,d, 6a,b, 6d_DCM, 7a,b, 8, and 9[a]

	1a[b] X = S(1) Y = S(2)	1d X = S(1) Y = S(2)	6a X = Se(1) Y = Se(2)	6b X = Se(1) Y = Se(2)	6d_DCM X = Se(1) Y = Se(2)	7a X = S(1) Y = Se(1)	7b X = S Y = Se	8 X = S(1) Y = S(2)	9 X = Se(1) Y = Se(2)
Fe(1)−Fe(2)	2.506(1)	2.536(3)	2.5482(8)	2.5617(13)	2.5734(17)	2.5270(10)	2.545(3)	2.5094(15)	2.5575(9)
Fe(1)−X	2.254(1)	2.252(4)	2.3606(7)	2.3484(12)	2.3513(15)	2.271(5)	2.28(6)	2.2444(18)	2.3584(7)
Fe(1)−Y	2.248(1)	2.237(4)	2.3632(7)	2.3668(11)	2.3621(14)	2.377(3)	2.338(14)	2.241(2)	2.3555(8)
Fe(2)−X	2.255(1)	2.247(4)	2.3601(7)	2.3556(12)	2.3573(15)	2.215(5)	2.21(4)	2.249(2)	2.3509(7)
Fe(2)−Y	2.249(1)	2.253(5)	2.3664(7)	2.3500(12)	2.3584(14)	2.367(3)	2.334(13)	2.246(2)	2.3514(7)
Fe(1)−C(11)	1.788(3)	1.85(2)	1.804(4)	1.803(8)	1.807(10)	1.799(5)	1.805(14)	1.802(7)	1.789(5)
Fe(1)−C(12)	1.797(3)	1.809(15)	1.803(4)	1.812(7)	1.802(10)	1.796(5)	1.792(14)	1.802(7)	1.802(4)
Fe(1)−C(13)	1.805(3)	1.819(16)	1.793(4)	1.799(7)	1.793(9)	1.805(5)	1.797(14)	1.805(7)	1.797(5)
Fe(2)−C(14)	1.801(3)	1.815(16)	1.798(4)	1.796(8)	1.788(9)	1.795(5)	1.843(14)	1.815(7)	1.807(5)
Fe(2)−C(15)	1.801(3)	1.791(16)	1.791(4)	1.811(8)	1.784(9)	1.790(5)	1.791(14)	1.805(7)	1.800(4)
Fe(2)−C(16)	1.805(4)	1.803(15)	1.800(4)	1.803(7)	1.798(10)	1.814(6)	1.820(15)	1.792(7)	1.803(4)
X−C(1)	1.777(3)	1.774(14)	1.911(4)	1.936(6)	1.924(8)	1.796(6)	1.83(6)	1.790(6)	1.917(4)
Y−C(8)	1.778(3)	1.774(12)	1.921(4)	1.955(7)	1.920(8)	1.886(5)	1.902(19)	1.769(6)	1.921(4)
X−Fe(1)−Y	84.12(3)	84.34(15)	85.08(2)	83.43(4)	85.85(5)	83.80(14)	83.1(12)	84.24(7)	84.97(3)
X−Fe(2)−Y	84.08(3)	84.09(14)	85.02(2)	83.63(4)	85.80(5)	85.26(13)	84.9(15)	84.03(7)	85.23(2)
X−C(1)−C(9)	125.3(2)	124.5(9)	126.7(3)	122.8(5)	127.2(6)	125.0(4)	121(2)	125.8(5)	127.8(3)
Y−C(8)−C(9)	125.4(2)	127.8(9)	126.7(3)	121.8(5)	127.3(6)	128.6(4)	126.4(10)	125.9(5)	127.7(3)
C(8)−C(9)−C(1)	125.4(3)	123.8(12)	126.2(4)	126.9(6)	125.8(8)	124.6(4)	124.5(12)	124.1(5)	124.2(4)
X−C(1)···C(8)−Y	−1.97(16)[c]	−0.8(7)	2.32(19)	25.0(3)	3.1(5)	3.6(3)	−18.8(18)	2.2(3)	−1.8(2)
X···Y	3.0159(10)[c]	3.013(5)	3.1939(6)	3.1374(9)	3.2101(12)	3.105(6)	3.07(5)	3.008(3)	3.1836(8)
angle between planes 1 and 2[d]	93.21(4)	92.4(2)	93.46(5)	68.91(9)	89.42(12)	93.51(6)	71.4(2)	89.00(8)	88.20(5)

[a]Where there are two crystallographically independent molecules (**7b**, **8**, and **9**) only data from one molecule are given. Where there is disorder in the X and Y groups (**7a**,**b**), only the parameters from the major component are given. In both cases, the parameters that are not shown are entirely comparable with those that are given (see the Supporting Information for tabulated values). [b]Data taken from ref 4, CCDC 723538. [c]Distances calculated by the authors of this submission. [d]Plane 1 is the least-squares plane through C(1)−C(10). Plane 2 is the least-squares plane through Fe(1), Fe(2), and the two "in-line" carbonyl groups, (C(13), O(3), C(16), O6) in **1a**; C(11), O(1), C(16), O(6) in **6a** and **7a**; C(11), O(1), C(14), O(4) in **1d**, **6b**, **6d_DCM**, **7b**, **8**, and **9**).

(except for **1d** and **9**) is closer to reversible. It has been suggested that the first reduction wave results in a small structural rearrangement,[37] which would both slow electron transfer kinetics and result in a reduced amplitude of the return wave. This rearrangement is unlikely to involve fragmentation of the backbone because an oxidation peak is observed on the return sweep.[7] The oxidation peak currents are difficult to measure because of the difficulty in determining the baseline but in some cases (e.g., compounds **6a**,**b**,**d**, **7a**,**b**) the ratio of oxidation and reduction peak heights increases on increasing scan rate, indicating that such an EC (electrochemical chemical) reaction does take place. With the exception of complex **9**, the product of the second reduction appears more stable (on the time scale of the experiment), which is likely to result from a slower chemical decomposition of that reduction product.

Although accurate determination of $E_{1/2}$ values in this type of reaction is difficult it is possible to make qualitative comparisons. Considering compound **1d** in relation to compounds **1a** and **1b**, it can be seen that **1b** has the most negative $E'_{1/2}$ for the first reduction process and **1d** has a more negative $E'_{1/2}$ than **1a**. A more negative $E_{1/2}$ indicates that the reduction is thermodynamically less favorable; the electron donating −OMe groups and *t*-Bu groups destabilize the reduced form of the complex relative to **1a**. The products of the electrochemical reduction appear stable, which has been explained for **1a**−**c** to be a result of partial delocalization of the negative charges on the aromatic backbone and a degree of rigidity that prevents dimerization of the reduced forms or fragmentation of the complex.[4]

Surprisingly, the replacement of the sulfur atoms with selenium results in a positive shift in reduction potential for each complex **a**, **b**, **d**. The effect of selenium on reduction potential cannot be rationalized by considering its effect on electron density on the iron centers. As seen in the IR data, selenium increases this electron density relative to the equivalent sulfur complex. The higher electron density on the iron centers should make the reduction process thermodynamically less favorable, which would, in turn, cause the reduction to proceed at a more negative potential.[8] Complex **6d** is reduced at more negative potentials than **6a**, similar behavior to complexes **1d** and **1a**. However, the first reduction of compound **6b** occurs at a more positive potential than that of **6a**, which is the opposite trend to that observed for **1a** and **1b**. The twisted conformation of **6b**, evident in the X-ray crystal structure, could contribute to the ease of reduction. The reduction products of the selenolate-based complex **6d** appear less stable than those of the thiolate-based complex **1d**, in that the oxidation peak current (particularly for **6d**) appears smaller than the reduction peak current. Assuming that the diffusivities of the oxidized and reduced forms of the complex are similar, a difference in peak height suggests decomposition of the reduced product, in an EC reaction. Thus, although the incorporation of selenium facilitates the reduction of the iron centers, it has an adverse effect on the complex stability under reducing conditions.

The thiaselenolate-based complexes, **7a** and **7b**, exhibit reduction waves for the first process in between those of the corresponding disulfur and diselenium complexes, consistent with previous reports.[8,15,17,20] Interestingly, the peak positions

dx.doi.org/10.1021/om500683p | Organometallics 2014, 33, 4449−4460

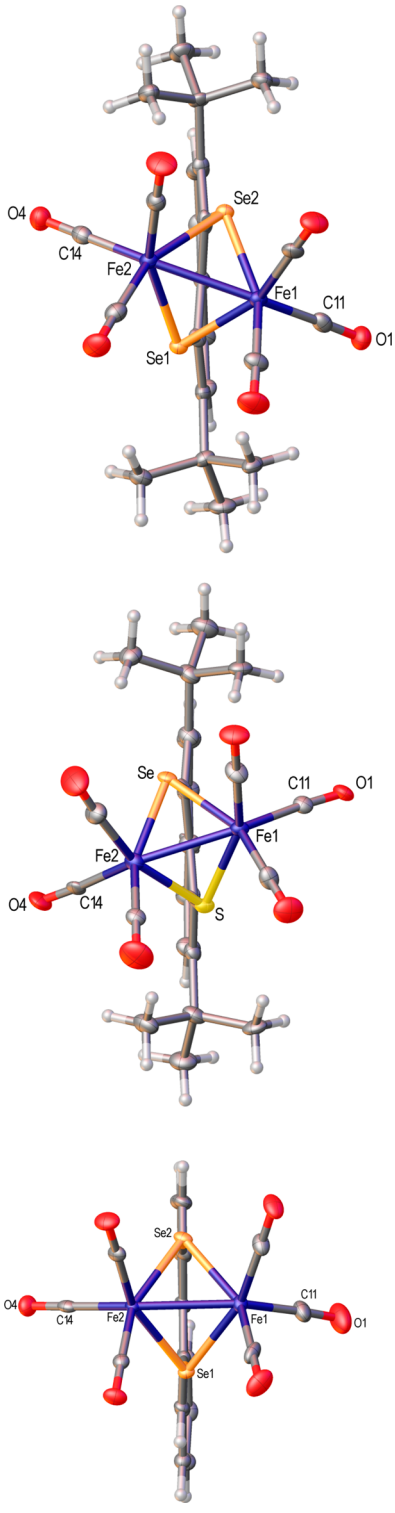

Figure 6. Projections of the alignment of the plane through C(1)–C(10) (plane 1) and the plane through Fe(1), Fe(2) and the two "in-line" carbonyl groups, C(11), O(1), C(14), O(4), in [FeFe]-complexes **6b** (top) and **7b** (middle) and **9** (bottom).

observed for **7a** and **7b** are similar, despite the twisted conformation of **7b**. However, the oxidation behavior differs, with the oxidation peak position of **7a** being substantially more negative than that of **7b**.

The phenanthrene-1,10-dithiolate-based complex **8** exhibits a reduction wave at −1.51 V, negative of the corresponding process for compound **1a**. In contrast, the reduction of [(μ-PNT)$Fe_2(CO)_6$] (**2** in Figure 2)[7] occurs at a less negative potential than that of the naphthalene equivalent **1a**. Comparison of the behavior of **8** with **2** demonstrates that the addition of an aromatic ring does not necessarily increase stabilization of the reduced form of the complex; rather, the nature of the linkage of the [FeFe]-cluster unit is also important in determining electrochemical properties. The diselenolate equivalent, **9**, has a reduction wave centered at −1.39 V, more positive than that of **8**, in line with the trends observed for the naphthalene-based complexes. However, the $E_{1/2}$ is more positive for **9** than for **6a**, indicating that the additional ring does confer relative stability on the reduced form of the complex in this case. The second reduction process is less well-defined for complex **9**, which might suggest a lack of stability of the second reduction product. As suggested for **2**,[7] structural rearrangements of the reduced forms of these complexes might take place, resulting in a lack of reversibility of the redox processes.

Proton Reduction Catalysis. Complexes **1d**, **6a**,**b**,**d**, **7a**,**b**, **8**, and **9** have been tested as proton reduction electrocatalysts by monitoring their electrochemical properties on addition of *p*-TsOH acid (pK_a = 8 in acetonitrile, concentrations 2.5–10 mM).[38] The CVs are shown in Figures 9 and S8 (Supporting Information). In previously reported studies on Fe–porphyrin complexes, it was observed that upon raising the concentration of acid, the first reduction wave was shifted toward more negative potentials and that the peak current (I_{pc}) increased linearly as a function of the acid concentration. The reduction process also became irreversible.[39] This behavior is typical of catalytic processes, where the reaction is fast and the current is controlled by the diffusion of the molecules at the electrode's surface.[40,41] The interpretation was that a monoanion is formed during the first one-electron reduction and then reacts rapidly with protons before subsequently being reduced by a second one-electron reduction. This species in turn combines with a proton to afford molecular hydrogen.

Complexes **1d**, **6a**, and **8** do not display this catalytic behavior, but instead, a new reduction wave appears upon addition of *p*-TsOH, between the first and the second reduction peaks, and this wave does not have any anodic counterpart. Its intensity increases with the acid concentration. In order to exclude any contribution of the working electrode to the proton reduction,[42,43] the same experiment was performed in the absence of catalyst (shown in Figure S9, Supporting Information).[44a] The proton reduction at the glassy carbon electrode in the absence of catalyst occurs at more negative potentials than the peaks observed in the presence of the catalysts and the reduction peaks are broader. Hence, the new peak does not correspond to proton reduction at carbon but is instead indicative of a different mechanism from that observed for the Fe-porphyrin catalysts.[39] The results that have been reported for complexes **1a** and **1b** are similar to our results for complex **1d** measured under the same conditions. The second new reduction wave for complex **1b** was assigned by Tilley et al. to an intermediate that was not identified experimentally.[4] Scheme 3 shows their suggested mechanism, based on an original proposal by Pickett.[45] As in the case for Fe–porphyrins, the first reduction wave corresponds to the formation of the first monoanion and its rapid reaction with the acid forming a protonated neutral species (e.g., **1aH**), which can then be further reduced to form $\mathbf{1aH}^-$. This species is rapidly protonated a second time, leading to $\mathbf{1aH_2}$. $\mathbf{1aH_2}$ can

dx.doi.org/10.1021/om500683p | *Organometallics* 2014, 33, 4449–4460

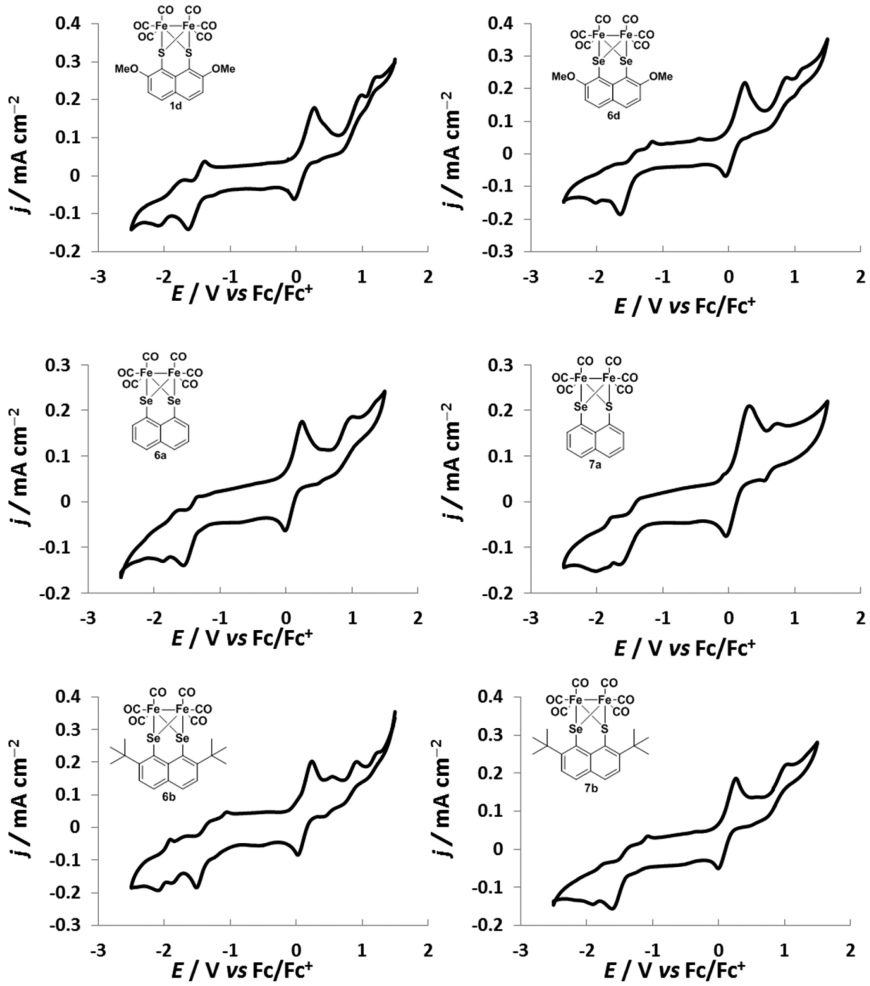

Figure 7. Cyclic voltammograms for [FeFe]-complexes **1d**, **6a**,**b**,**d** and **7a**,**b** (1 mM) in 0.1 M NBu_4PF_6/CH_3CN at 0.01 V s^{-1} scan rate.

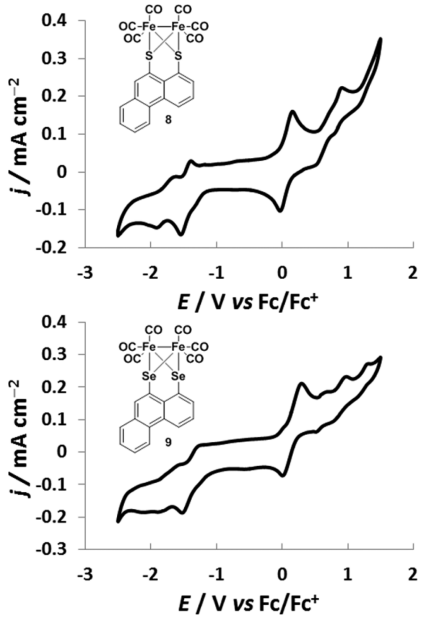

Figure 8. Cyclic voltammograms for [FeFe]-complexes **8** and **9** (1 mM) in 0.1 M NBu_4PF_6/CH_3CN at 0.01 V s^{-1} scan rate.

then liberate molecular hydrogen and release the complex **1a** or can be further reduced to $\mathbf{1aH_2}^-$, which liberates molecular hydrogen and releases the reduced form of the complex, $\mathbf{1a}^-$.[44] Thus, three different reduction waves are possible. Based on these findings, we can surmise that complexes **1d**, **6a** and **8** undergo this type of proton reduction cycle, which involves two distinct reduced/protonated species. The new reduction wave of **1d** and **6a** appears at concentrations of 5 mM of *p*-TsOH and above but for complex **8** only above 7.5 mM of acid. The dependence of this new wave on acid concentration is suggestive of a parallel mechanism, such as that proposed by Tilley et al., and that one pathway is favored by high acid concentration. It is also possible that protons are associated only with the dianion produced in the second reduction process but this behavior was shown to occur only with weaker acids than *p*-TsOH. In the presence of *p*-TsOH, it is more likely that the protonation step of the monoanion is rapid.

Upon addition of 2.5 mM of *p*-TsOH, complex **7a** displays a first reduction wave at −1.28 V, which could be assigned to both the first one-electron reduction and following protonation, while the second wave at −1.54 V leads to the formation of molecular hydrogen. Upon increasing the concentration of acid, **7a** and **7b** follow the catalytic pathway of **1d**. Apparently, the higher electron density of the Fe centers in compounds **6b** and **6d** encourages the liberation of hydrogen after the second reduction step or the complex is not able to be further reduced, whereas **1d**, with two S atoms, requires a further reduction step before liberating hydrogen. The S−Se complexes **7a** and **7b**

dx.doi.org/10.1021/om500683p | *Organometallics* 2014, 33, 4449−4460

Table 3. Electrochemical Reduction Potentials (vs Fc/Fc^+) [FeFe]-Complexes 1d, 6a,b,d, 7a,b, 8, and 9 (1 mM) in 0.1 M NBu_4PF_6/CH_3CN at 0.01 V s^{-1} Scan Rate

complex	E'_{pc}[a] (V)	$E'_{1/2}$[a] $Fe^IFe^I \rightarrow Fe^IFe^0$ (V)	E''_{pc} (V)	$E''_{1/2}$ $Fe^IFe^0 \rightarrow Fe^0Fe^0$ (V)	E_{pa} (V)	$(E_{1/2} - E^\circ_{p\text{-TsOH}})$ (V)
1a[b]	−1.52	−1.48	−1.96		0.87	0.83
1b[b]	−1.59	−1.55	−2.05		0.78	0.90
1d	−1.65	−1.52	−2.08	−1.92	0.99	0.87
					1.20	
6a	−1.54	−1.44	−1.86	−1.75	1.00	0.79
6b	−1.34	−1.41	−2.15	−2.01	0.55	0.76
					0.90	
6d	−1.64	−1.50	−2.02	−1.90	0.88	0.85
					1.13	
7a	−1.60	−1.47	−1.91	−1.82	0.68	0.82
					1.12	
7b	−1.61	−1.48	−1.90	−1.82	1.07	0.83
8	−1.64	−1.51	−2.02	−1.84	0.87	0.86
					1.14	
9	−1.52	−1.39			0.98	0.74
					1.31	

[a]Values derived from CV over limited potential range avoiding second reduction wave. [b]Data taken from ref 4.

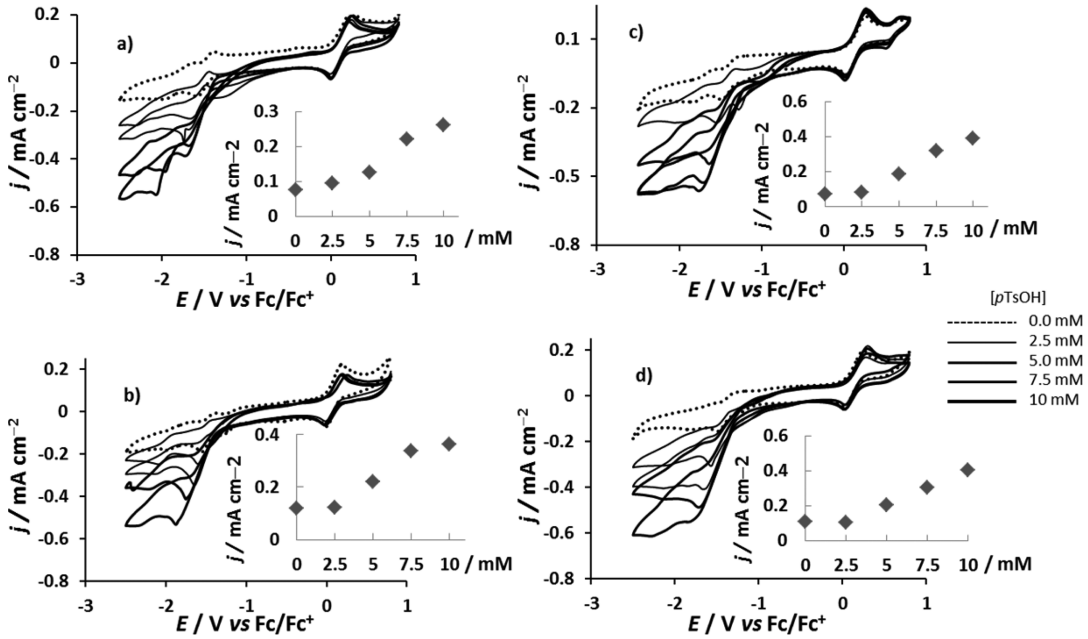

Figure 9. Cyclic voltammograms for [FeFe]-complexes **1d** (a), **6d** (b), **7a** (c), and **9** (d) (1 mM) in 0.1 M NBu_4PF_6/CH_3CN at 0.01 V s^{-1} scan rate with increasing concentrationc of *p*-TsOH (from 2.5 M to 10 mM). The insets show the linear proportionality between the increase of the current density (j) and the concentration of the acid ([TsOH]) during the proton reduction catalysis.

Scheme 3. Mechanism Proposed by Tilley for Catalysis of pTSA Proton Reduction[4]

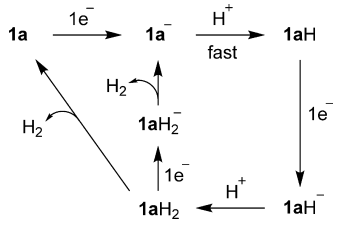

apparently show both reaction pathways, depending on acid concentration.

The efficacy of the catalysts can be evaluated by considering the increase in current on addition of acid and also the potentials required to drive the reaction. Evans calculated the standard potential for many different acids which are used to test the electrocatalytic activity of synthetic mimics of [FeFe]-hydrogenase, which depends in each case on the pK_a and the solvent.[43] The standard potential for *p*-TsOH proton reduction in acetonitrile is −0.65 V vs Fc/Fc^+. If proton reduction occurs at the same potential as the reduction of the catalyst, the difference between the catalyst's half-wave potential and −0.65 V provides a measure of the decrease in activation energy for the reaction in the presence of a catalyst. These values are reported in Table 3 for complexes **1d**, **6a,b,d**, **7a,b**, **8**, and **9**. The values for the diselenolate-based [FeFe]-complexes are lower, indicating that they are more efficient proton reduction electrocatalysts than the corresponding dithiolates, whose values are comparable with those reported in the literature.[4,7]

dx.doi.org/10.1021/om500683p | *Organometallics* 2014, 33, 4449−4460

The current intensity/acid concentrations proportionality (insets to Figures 9 and S8, Supporting Information) demonstrate that complexes **1d**, **6a**,**b**,**d**, **7a**,**b**, **8**, and **9** are catalysts for proton reduction. The selenium-containing complexes all give larger slopes than complexes containing sulfur alone. For example, comparing the catalytic activity of **1d** and **6d** (Figure S10, Supporting Information), the diselenolate-based [FeFe]-complex **1d** is a more effective proton reduction catalyst than the corresponding dithiolate **1d** in terms of current produced during the reaction.

CONCLUSION

These studies have investigated the rôle of the chalcogen and the aromatic backbone in determining the properties of [FeFe]-complexes. Electrochemical studies showed that naphthalene and phenanthrene-based dichalcogen ligands confer increased stability to the reduced diiron complexes compared with saturated ligand backbones. The reduction of the diselenolate-based [FeFe]-complexes (**6a**,**b**,**d** and **9**) occurred at less negative potentials than those of the corresponding dithiolates (**1a**,**b**,**d** and **8**), which led to a decrease in overpotential for proton reduction. This observation, combined with the larger currents measured during proton reduction, demonstrated that the diselenolate-based complexes catalyzed proton reduction more efficiently. However, the diselenolate-based complexes are less stable upon electrochemical reduction than the corresponding dithiolates.

EXPERIMENTAL SECTION

Synthesis. Solvents and reagents were purified as follows: *n*-BuLi was purchased as either 2.5 or 1.6 M solutions in hexane and the solutions titrated with menthol in the presence of 1-(biphenyl-4-yl)-3-phenyl-2-azapropene ("BLUE"). TMEDA was distilled from calcium hydride. *p*-Toluenesulfonic acid monohydrate was purchased from Aldrich, dehydrated by heating at 100 °C for 4 h under vacuum and recrystallized from $CHCl_3$.[45] Dry solvents were obtained and purified using a Pure Solv-MD solvent purification system and were transferred under argon. All other reagents and solvents were purchased and used as received from commercial sources. The following cooling baths were used: 0 °C (ice/water) and −78 °C (dry ice/acetone). All reactions in nonaqueous solvents were carried out under argon in oven-dried glassware. Melting points were determined using open glass capillaries on a Gallenkamp melting point apparatus and are uncorrected. Analytical TLC was carried out on Merck 60 F245 aluminum-backed silica gel plates. Short wave UV (245 nm) and $KMnO_4$ were used to visualize components. Compounds were purified by flash column chromatography using Merck silica gel 60.

Naphtho[1,8-*cd*][1,2]diselenole (**11a**),[27,28] 2,7-di-*tert*-butylnaphtho-[1,8-*cd*][1,2]diselenole (**11b**),[22,28] 2,7-dimethoxynaphtho[1,8-*cd*]-[1,2]diselenole (**11d**),[29] naphtho[1,8-*cd*][1,2]thiaselenole (**12a**),[30−32] 2,7-dimethoxynaphtho[1,8-*cd*][1,2]dithiole (**10d**),[23] and phenanthro-[1,10-*cd*][1,2]dithiole (**13**)[33] were synthesized according to literature procedures.

Spectroscopy. ^1H and ^{13}C NMR data were recorded on a Bruker AVIII300, a Bruker AVIII400, or a Bruker AV400 spectrometer. Spectra were recorded in deuterochloroform referenced to residual $CHCl_3$ (^1H, 7.26 ppm; ^{13}C, 77.2 ppm)[46] and in DMSO-d_6 referenced to residual DMSO (^1H, 2.50 ppm; ^{13}C, 39.5 ppm). Chemical shifts (δ) are reported in ppm and coupling constants (J) are reported in hertz. The following abbreviations are used to describe multiplicity: s, singlet; d, doublet; t, triplet; q, quartet; m, multiplet; b, broad; ap, apparent. All coupling constants are reported and averaged. Mass spectra were recorded on a LCT spectrometer utilizing electrospray ionization (recorded in the positive mode) with a methanol mobile phase, or electron impact ionization, and are reported as m/z (%). HRMS were recorded on a LCT spectrometer using lock mass incorporated into the mobile phase. IR spectra were recorded on a Perkin-Elmer Spectrum 100 FT-IR spectrometer. UV/vis spectra were recorded on a Cary 50 Scan UV−vis spectrometer.

X-ray Crystallography. Crystals were obtained by slow evaporation of dichloromethane solutions. Suitable crystals were selected and data sets were measured on an Agilent SuperNova diffractometer equipped with an Atlas detector for **6a**, **7a**, and **9** ($\lambda_{Cu-K\alpha}$ = 1.5418 Å) and for **6d_DCM** (($\lambda_{Mo-K\alpha}$ = 0.71073 Å) and by the EPSRC UK National Crystallography Service[47] on a Rigaku AFC12 goniometer equipped with an enhanced sensitivity (HG) Saturn724+ detector mounted at the window of an FR-E+ SuperBright molybdenum rotating anode generator ($\lambda_{Mo-K\alpha}$ = 0.71073 Å) with HF Varimax optics for **1d**, **6b**, **7b**, and **8**. Both instruments were equipped with an Oxford Cryosystems Cryostream device with diffraction data collected at 100 K in all cases. Absorption corrections were applied using CrysAlisPro[48] for **6a**, **6d_DCM**, **7a** and **9**, using a numerical absorption correction based on Gaussian integration over a multi-faceted crystal model for **6a**,**6d_DCM**, and **9** and an empirical absorption correction using spherical harmonics implemented in SCALE3 ABSPACK scaling algorithm for **7a**. Empirical absorption corrections were applied using CrystalClear-SM Expert[49] for **1d**, **6b**, **7b**, and **8**. The structures were solved by direct methods in SHELXS-97[50] for **1d**, **6a**,**b**, **7a**, and **8** in SHELXS-2013[50] for **7b** and **9** and in SHELXS-2014[50] for **6d_DCM** and all were refined by a full-matrix least-squares procedure on F^2 in SHELXL-2013 (SHELXL-2014 for **6d_DCM**).[50] All non-hydrogen atoms were refined with anisotropic displacement parameters apart from disordered atoms in **7a** (see later comments). The hydrogen atoms were added at calculated positions and refined by use of a riding model with isotropic displacement parameters based on the equivalent isotropic displacement parameter (U_{eq}) of the parent atom. Figures were produced and some structural analysis was carried out using OLEX2.[51] CCDC-996634−996636, 996638−996641, and 1008312 contain the supplementary crystallographic data for **1d**, **6a**,**b**, **7a**,**b**, **8**, **9**, and **6d_DCM**, respectively. These data can be obtained free of charge from the Cambridge Crystallographic Data Centre via http://www.ccdc.cam.ac.uk/Community/Requestastructure/pages/Requestastructure.aspx.

1d: Although every effort was made to grow the best possible crystals, the quality of the crystals and thus corresponding diffraction data was poor. It was necessary to choose a thin platelet in order to obtain a single crystal, and this did not diffract well to higher angles.

6b: The crystal was a merohedral twin with the two domains related by 180° about the direct axis [1 0 0]. The scale factor relating the two domains is 0.12.

7a: The sulfur and selenium atoms are both disordered over two positions, with the refined percentage occupancy ratio between the major and minor positions (labeled Se/S and S′/Se′ respectively), being 69.8(3):30.2(3). The minor components, S′ and Se′, were refined isotropically because of their relatively low occupancy.

7b: The structure contains two crystallographically independent molecules, with the corresponding geometric parameters being entirely comparable. The sulfur and selenium atoms in both molecules are both disordered over two positions, with the refined percentage occupancy ratio between the major and minor positions (labeled Se/S and S′/Se′ in molecule 1 and Se1/S1 and S1′/Se1′ in molecule 2, respectively), being 51.1(8):48.9(8) (molecule 1) and 53.0(8):47.0(8) (molecule 2).

8: The structure contains two crystallographically independent molecules, with the corresponding geometric parameters being entirely comparable.

9: The structure contains two crystallographically independent molecules, with the corresponding geometric parameters being entirely comparable. In molecule 2 the carbonyl ligand C116, O106/C16′, O16′ is disordered over two positions with the refined percentage occupancy ratio being 57.4(12):42.6(12).

Electrochemistry. Electrochemical studies were performed with a CHI601B electrochemical analyzer (CH Instruments). All measurements were carried out under argon at room temperature in dry CH_3CN. Tetrabutylammomiun hexafluorophosphate (NBu_4PF_6, 0.1 M in CH_3CN) was used as supporting electrolyte. A conventional

dx.doi.org/10.1021/om500683p | *Organometallics* 2014, 33, 4449−4460

three-electrode system was employed. The working electrode was a glassy carbon electrode (diameter: 1.0 mm). Silver/silver nitrate (Ag/$AgNO_3$, 10 mM solution in CH_3CN) was used as an external reference electrode and a platinum wire was used as auxiliary electrode. Ferrocene was used as an internal reference. All potentials reported in this work are with reference to the Fc/Fc^+ couple. All cyclic voltammograms were carried out at a scan rate of 0.01 V s^{-1}.

All glassware was cleaned using a 1:1 mixture of ammonia and hydrogen peroxide followed by thorough rinsing with pure water. Glassware was soaked in pure water for 12 h and then rinsed and oven-dried overnight. Water used throughout (including solution preparation and rinsing) was purified by a Millipore system (resistivity 18.2 MΩ cm, TOC ≤ 5 ppb). The working electrode was prepared by polishing with aqueous slurries of successively finer grades of alumina powder (1, 0.3, and 0.05 μm, Buehler), followed by rinsing and placing in pure water in an ultrasonic bath for several min, then drying in a stream of argon.

[$Fe_2(CO)_6$(1,8-S_2-2,7-OMe-$C_{10}H_4$)] (**1d**). A solution of 3,8-dimethoxynaphtho[1,8-*cd*][1,2]dithiole (**15**) (0.20 g, 0.80 mmol) and $Fe_3(CO)_{12}$ (0.40 g, 0.80 mmol) in toluene (17 mL) was refluxed for 4 h under an argon atmosphere. The mixture was cooled to room temperature, filtered, and concentrated under reduced pressure. The residue was purified by column chromatography (9:1, hexane/EtOAc) to give complex **1d** (0.37 g, 69%) as a red crystalline solid: R_f 0.13 (9:1, hexane/EtOAc); mp >160 °C dec; λ_{nm} (MeCN) 361 (ε = 5.7 × 10^3 M^{-1} cm^{-1}), 327 (ε = 6.1 × 10^3 M^{-1} cm^{-1}), 237 (ε = 1.6 × 10^4 M^{-1} cm^{-1}); ν_{max} (solid state, ATR)/cm^{-1} 2061 (CO), 2021 (CO), 1976 (CO), 1955 (CO), 1878 (CO); δ_H (400 MHz, $CDCl_3$) 4.10 (6 H, s, OCH_3), 7.15 (2 H, d, *J* = 9.0 Hz, Ar*H*), 7.90 (2 H, d, *J* = 9.0 Hz, Ar*H*); δ_C (101 MHz, $CDCl_3$) 57.2 (2 × CH_3), 108.7 (2 × C), 110.3 (2 × CH), 124.5 (C), 129.9 (C), 132.9 (2 × CH), 160.0 (2 × C), 208.2 (6 × C); *m*/*z* (EI^+) 525.8586 ([M +Na]$^+$, $C_{18}H_{10}O_8S_2{}^{56}Fe_2Na$ requires 525.8609) 390 (100%, M^+ − 4CO), 418 (52, M^+ − 3CO), 446 (41, M^+ − 2CO), 474 (34, M^+ − CO), 502 (50, M^+), 530 (20). Anal. Calcd for $C_{18}H_{10}Fe_2O_8S_2$: C, 40.78; H, 1.90. Found: C, 40.56; H, 1.88.

[$Fe_2(CO)_6$(1,8-Se_2-$C_{10}H_6$)] (**6a**). A solution of naphtho[1,8-*cd*][1,2]-diselenole (**11a**) (0.08 g, 0.28 mmol) and $Fe_3(CO)_{12}$ (0.14 g, 0.28 mmol) in toluene (7.5 mL) was refluxed for 2.5 h under an argon atmosphere. The mixture was cooled to room temperature, filtered, and concentrated under reduced pressure. The residue was purified by column chromatography (hexane) to afford complex **6a** (0.15 g, 96%) as a dark red solid: R_f 0.47 (hexane); mp >130 °C dec; λ_{nm} (MeCN) 345 (ε = 5.4 × 10^3 M^{-1} cm^{-1}); ν_{max} (solid state, ATR)/cm^{-1} 2058 (CO), 2016 (CO), 1996 (CO), 1979 (CO), 1822 (CO); δ_H(400 MHz, $CDCl_3$) 7.40 (2 H, t, *J* = 9.0 Hz, Ar*H*), 7.99 (2 H, d, *J* = 9.0 Hz, Ar*H*), 8.29 (2 H, d, *J* = 9.0 Hz, Ar*H*); δ_C (101 MHz, $CDCl_3$) 119.2 (2 × C), 125.4 (2 × CH), 128.9 (C), 132.9 (2 × CH), 134.2 (C), 134.9 (2 × CH), 208.6 (6 × C); *m*/*z* (EI^+) 565.7173 (M^+, $C_{16}H_6O_6{}^{56}Fe_2{}^{80}Se_2$ requires 565.7193), 564 (100), 557 (8), 560 (43), 561 (19), 562 (82), 563 (9), 565 (9). Anal. Calcd for $C_{16}H_6O_6Fe_2Se_2$: C, 34.08; H, 1.07. Found: C, 34.14; H, 1.01.

[$Fe_2(CO)_6$(1,8-Se_2-2,7-di-tert-butyl-$C_{10}H_4$)] (**6b**). A solution of 2,7-di-*tert*-butylnaphtho[1,8-*cd*][1,2]diselenole (**11b**) (0.15 g, 0.39 mmol) and $Fe_3(CO)_{12}$ (0.18 g, 0.39 mmol) in toluene (14 mL) was refluxed for 4 h under an argon atmosphere. The mixture was cooled to room temperature, filtered, and concentrated under reduced pressure. The residue was purified by column chromatography (hexane) to afford complex **6b** (0.12 g, 44%) as a dark orange solid: R_f 0.50 (hexane); mp >150 °C dec; λ_{nm} (MeCN) 346 (ε = 1.3 × 10^4 $M^{-1}cm^{-1}$); ν_{max} (solid state, ATR)/cm^{-1} 2057 (CO), 2015 (CO), 1979 (CO), 1970 (CO), 1956 (CO); δ_H (400 MHz, $CDCl_3$) 1.83 (18 H, s, *t*Bu), 7.66 (2 H, d, *J* = 8.5 Hz, Ar*H*), 7.75 (2 H, d, *J* = 8.5 Hz, Ar*H*); δ_C (101 MHz, $CDCl_3$) 33.5 (6 × CH_3), 39.7 (2 × C), 118.8 (2 × C), 125.1 (2 × CH), 131.0 (2 × CH), 131.1 (C), 133.0 (C), 154.0 (2 × C), 208.8 (6 × C, CO); *m*/*z* (ES^+) 698.8378 ([M + Na]$^+$, $C_{24}H_{22}O_6Na^{56}Fe_2{}^{78}Se^{80}Se$ requires 698.8351), 702 (100), 698 (61), 699 (42), 700 (99), 701 (35), 703 (30), 704 (35). Anal. Calcd for $C_{24}H_{22}Fe_2O_8Se_2$: C, 42.64; H, 3.28. Found: C, 42.85; H, 3.21.

[$Fe_2(CO)_6$(1,8-Se_2-2,7-OMe-$C_{10}H_4$)] (**6d**). A solution of 2,7-dimethoxynaphtho[1,8-*cd*][1,2]diselenole (**11d**) (0.35 g, 1.01 mmol) and $Fe_3(CO)_{12}$ (0.51 g, 1.01 mmol) in toluene (28 mL) was refluxed for 4 h under an argon atmosphere. The mixture was cooled to room temperature, filtered, and concentrated under reduced pressure. The residue was purified by column chromatography (8:2, hexane/EtOAc) to afford complex **6d** (0.30 g, 47%) as a red crystalline solid: R_f 0.13 (8:2, hexane/EtOAc); mp >140 °C dec; λ_{nm} (MeCN) 358 (ε = 3.1 × 10^3 $M^{-1}cm^{-1}$), 336 (ε = 3.7 × 10^3 $M^{-1}cm^{-1}$), 237 (ε = 1.6 × 10^4 $M^{-1}cm^{-1}$); ν_{max} (solid state, ATR)/cm^{-1} 2054 (CO), 2014 (CO), 1970 (CO), 1950 (CO), 1875 (CO); δ_H (400 MHz, $CDCl_3$) 4.08 (6 H, s, OCH_3), 7.13 (2 H, d, *J* = 6.0 Hz, Ar*H*), 7.85 (2 H, d, *J* = 6.0 Hz, Ar*H*); δ_C (101 MHz, $CDCl_3$) 57.3 (2 × CH_3), 103.6 (2 × C), 110.1 (2 × CH), 124.7 (C), 131.8 (C), 133.4 (2 × CH), 160.0 (2 × C), 209.0 (6 × C, CO). Anal. Calcd for $C_{18}H_{10}Fe_2O_8Se_2$: C, 34.65; H, 1.62. Found: C, 35.15; H, 1.73.

[$Fe_2(CO)_6$(1,8-SeS-$C_{10}H_6$)] (**7a**). A solution of naphtho[1,8-*cd*][1,2]-thiaselenole (**12a**) (0.20 g, 0.84 mmol) and $Fe_3(CO)_{12}$ (0.43 g, 0.84 mmol) in toluene (22 mL) was refluxed for 4 h under an argon atmosphere. The mixture was cooled to room temperature, filtered, and concentrated under reduced pressure. The residue was purified by column chromatography (hexane) to afford complex **7a** (0.14 g, 32%) as a red crystalline solid: R_f 0.56 (hexane), mp >120 °C dec; λ_{nm} (MeCN) 348 (ε = 8.5 × 10^3 $M^{-1}cm^{-1}$); ν_{max} (solid state, ATR)/cm^{-1} 2061 (CO), 2020 (CO), 1999 (CO), 1982 (CO), 1958 (CO), 1822 (CO); δ_H (400 MHz, $CDCl_3$) 7.37−7.44 (2 H, m, Ar*H*), 7.98−8.02 (2 H, m, Ar*H*), 8.23 (1 H, d, *J* = 6.9 Hz, Ar*H*), 8.32 (1 H, d, *J* = 6.9 Hz, Ar*H*); δ_C (101 MHz, $CDCl_3$) 117.0 (C), 125.3 (CH), 125.4 (CH), 126.7 (C), 132.4 (CH), 133.6 (CH), 134.1 (CH), 134.2 (C), 208.2 (6 × C, CO); *m*/*z* (EI^+) 517.7740 (M^+, $C_{16}H_6O_6S^{56}Fe_2{}^{80}Se$ requires 517.7749) 349 (100, M^+ − 6CO), 377 (14, M^+ − 5CO), 405 (12, M^+ − 4CO), 433 (7, M^+ − 3CO), 461 (14, M^+ − 2CO), 517 (11, M^+). Anal. Calcd for $C_{16}H_6O_6SFe_2Se$: C, 37.18; H, 1.17. Found: C, 37.45; H, 1.30.

[$Fe_2(CO)_6$(1,8-SeS-2,7-di-tert-butyl-$C_{10}H_4$)] (**7b**). A solution of 2,7-di-*tert*-butylnaphtho[1,8-*cd*][1,2]thiaselenole (**12b**) (0.36 g, 1.02 mmol) and $Fe_3(CO)_{12}$ (0.51 g, 1.02 mmol) in toluene (27 mL) was refluxed for 4 h under an argon atmosphere. The mixture was cooled to room temperature, filtered, and concentrated under reduced pressure. The residue was purified by column chromatography (hexane) to afford complex **7b** (0.31 g, 47%) as a red crystalline solid: R_f 0.69 (hexane); mp 122−124 °C; λ_{nm} (MeCN) 351 (ε = 4.1 × 10^3 $M^{-1}cm^{-1}$), 309 (ε = 3.7 × 10^3 $M^{-1}cm^{-1}$); ν_{max} (solid state, ATR)/cm^{-1} 2061 (CO), 2017 (CO), 1980 (CO), 1972 (CO), 1961 (CO), 1940 (CO); δ_H (400 MHz, $CDCl_3$) 1.78 (9 H, s, *t*Bu), 1.81 (9 H, s, *t*Bu), 7.66 (2H, d, *J* = 8.0 Hz, Ar*H*), 7.80 (2 H, d, *J* = 8.0 Hz, Ar*H*); δ_C (101 MHz, $CDCl_3$) 32.7 (3 × CH_3), 33.4 (3 × CH_3), 39.1 (C), 39.6 (C), 116.6 (C), 125.0 (CH), 125.2 (CH), 125.4 (C), 131.0 (CH), 131.2 (C), 131.4 (C), 131.5 (C), 153.7 (C), 154.9 (C), 208.5 (6 × C); *m*/*z* (EI^+) 629.9018 (M^+, $C_{24}H_{22}O_6S^{56}Fe_2{}^{80}Se$ requires 629.9001), 490 (100, M^+ − 5CO), 518 (38, M^+ − 4CO), 546 (33, M^+ − 3CO), 574 (29, M^+ − 2CO), 630 (31, M^+). Anal. Calcd for $C_{24}H_{22}O_6SFe_2Se$: C, 45.82; H, 3.52. Found: C, 45.51; H, 3.42.

[$Fe_2(CO)_6$(1,8-S_2-$C_{14}H_8$)] (**8**). A solution of phenanthro[1,10-*cd*]-[1,2]dithiole (**13**) (0.11 g, 0.47 mmol) and $Fe_3(CO)_{12}$ (0.24 g, 0.47 mmol) in toluene (13 mL) was refluxed for 4.5 h under an argon atmosphere. The mixture was cooled to room temperature, filtered, and concentrated under reduced pressure. The residue was purified by column chromatography (hexane) to afford complex **8** (0.125 g, 51%) as a red solid: R_f 0.63 (hexane); mp >360 °C dec; λ_{nm} (MeCN) 346 (ε = 6.3 × 10^3 $M^{-1}cm^{-1}$); ν_{max} (solid state, ATR)/cm^{-1} 2065 (CO), 2028 (CO), 1978 (CO), 1957 (CO), 1946 (CO), 1936 (CO); δ_H (400 MHz, $CDCl_3$) 7.56 (1 H, t, *J* = 7.7 Hz, Ar*H*), 7.70 (2 H, m, Ar*H*), 7.92 (1 H, d, *J* = 7.3 Hz, Ar*H*), 8.29 (1 H, d, *J* = 7.3 Hz, Ar*H*), 8.63 (1 H, s, Ar*H*), 8.66 (1 H, s, Ar*H*), 8.86 (1 H, d, *J* = 8.1 Hz, Ar*H*); δ_C (101 MHz, $CDCl_3$) 122.1 (C), 123.4 (CH), 125.8 (CH), 126.0 (CH), 126.5 (C), 128.2 (CH), 128.3 (CH), 128.7 (CH), 130.4 (2 × C), 131.7 (C), 132.0 (C), 133.2 (CH), 134.5 (CH), 207.8 (6 x C); *m*/*z* (EI^+) 519.8473 (M^+, $C_{20}H_8O_6S_2{}^{56}Fe_2$ requires 519.8461), 352 (100, M^+ − 6CO), 380 (11, M^+ − 5CO), 408 (11, M^+ − 4CO), 464 (5, M^+

– 2CO), 492 (4, M^+ – CO), 520 (5, M^+). Anal. Calcd for $C_{20}H_8Fe_2O_6S_2$: C, 46.19: H, 1.45, Found: C, 46.18; H, 1.48.

*[$Fe_2(CO)_6$(1,8-Se_2-$C_{10}H_8$)] (**9**).* A solution of phenanthro[1,10-*cd*][1,2]diselenole (**14**) (0.09 g, 0.28 mmol) and $Fe_3(CO)_{12}$ (0.28 g, 0.28 mmol) in toluene (7 mL) was refluxed for 4 h under an argon atmosphere. The mixture was cooled to room temperature, filtered, and concentrated under reduced pressure. The residue was purified by column chromatography (hexane) to afford complex **9** (0.05 g, 26%) as a red solid: R_f 0.65 (hexane); mp >140 °C dec; λ_{nm} (MeCN) 341 (ε = 1.6 × 10^4 $M^{-1}cm^{-1}$); ν_{max} (solid state, ATR)/cm^{-1} 2055 (CO), 2021 (CO), 1996 (CO), 1976 (CO), 1962 (CO), 1942 (CO); δ_H (400 MHz, $CDCl_3$) 7.53 (1 H, t, *J* = 7.3 Hz, Ar*H*), 7.69 (2 H, m, Ar*H*), 7.90 (1 H, d, *J* = 7.0 Hz, Ar*H*), 8.33 (1 H, d, *J* = 6.8 Hz, Ar*H*), 8.64 (1 H, s, Ar*H*), 8.67 (1 H, s, Ar*H*), 8.86 (1 H, d, *J* = 5.8 Hz, Ar*H*); δ_C (101 MHz, $CDCl_3$) 116.1 (C), 120.6 (C), 123.3 (C), 125.8 (CH), 126.4 (CH), 127.6 (C), 128.2 (CH), 128.6 (CH), 130.1 (C), 131.5 (C), 132.1 (C), 134.6 (CH), 136.1 (CH), 208.6 (6 × C; *m*/*z* (EI^+) 613.7343 (M^+, $C_{20}H_8O_6{}^{56}Fe_2{}^{78}Se^{80}Se$ requires 613.7358), 530 (100, M^+ - 3 CO), 474 (74, M^+ – 4 CO), 476 (81), 532 (72), 558 (57, M^+ – 2CO), 560 (42), 614 (10, M^+). Anal. Calcd for $C_{20}H_8O_6Fe_2Se_2$: C, 39.13: H, 1.31. Found: C, 39.44; H, 1.23.

*3,5,6,8-Tetrachloronaphtho[1,8-cd][1,2]diselenole (**11c**).* NCS (0.56 g, 4.22 mmol) was added to a solution of naphtho[1,8-*cd*][1,2]diselenole (**11a**) (0.20 g, 0.70 mmol) in CH_2Cl_2 (9.5 mL) at room temperature. The reaction mixture was stirred for 16 h under an argon atmosphere, dry loaded onto silica (2.00 g), and purified by flash column chromatography (hexane) to afford the title compound (0.06 g, 21%) as a yellow solid: R_f 0.79 (hexane); mp 224–225 °C; ν_{max} (solid state, ATR)/cm^{-1} 1735, 1549, 1532, 1468, 1382, 1336, 1273, 1255; δ_H (400 MHz, DMSO-d_6, 50 °C) 7.75 (2 H, s); δ_C (101 MHz, DMSO-d_6, 50 °C) 122.1 (2 × C, Ar*H*), 125.6 (2 × C, Ar*H*), 127.0 (C), 128.7 (C), 130.7 (2 × CH), 141.6 (2 × C); *m*/*z* (EI^+) 421.7231 (M^+, $C_{10}H_2Cl_4{}^{80}Se_2$ requires 421.7241), 389 (100), 321 (42), 353 (43), 393 (36), 423 (95), 427 (39).

*2,7-Di-tert-butylnaphtho[1,8-cd][1,2]thiaselenole (**12b**).* $FeCl_3$ (0.04 g, 0.25 mmol) was added in one portion to a solution of *t*BuBr (0.29 mL, 2.53 mmol) and naphtho[1,8-*cd*][1,2]thiaselenole **12a** (0.30 g, 1.27 mmol) in CH_2Cl_2 (3.0 mL). The mixture was refluxed overnight, allowed to cool to room temperature, concentrated under reduced pressure, and purified by column chromatography (hexane) to give the title compound (0.25 g, 56%) as a dark orange crystalline solid: R_f 0.59 (hexane); mp 118–119 °C; ν_{max} (solid state, ATR)/cm^{-1} 2292, 2253, 2056, 2016, 1979, 1443, 1375; δ_H (400 MHz, $CDCl_3$) 1.37 (6 H, s, *t*Bu), 1.39 (3 H, s, *t*Bu), 1.44 (6 H, s, *t*Bu), 1.46 (3 H, s, *t*Bu), 7.24–7.36 (4 H, m, ArH); δ_C (101 MHz, $CDCl_3$) 28.9 (3 × CH_3), 31.4 (3 × CH_3), 36.1 (C), 36.3 (C), 122.7 (CH), 124.0 (CH), 125.7 (CH), 125.8 (CH), 134.1 (2 × C), 138.8 (C), 140.1 (C), 141.8 (C), 142.4 (C); *m*/*z* (EI^+) 350.0607 (M^+, $C_{18}H_{22}S^{80}Se$ requires 350.0607), 335 (100), 331 (17), 333 (53), 350 (76), 352 (17), 353 (16).

*Phenanthro[1,10-cd][1,2]diselenole (**14**).* *n*BuLi (1.20 mL of a 1.68 M solution in hexane, 1.94 mmol) and TMEDA (0.29 mL, 1.94 mmol) were added dropwise over 30 min to a suspension of 9-bromophenanthrene (0.50 g, 1.94 mmol) in hexane (10 mL) at −30 °C under an argon atmosphere. The yellow mixture was stirred for 1 h at −30 °C and then allowed to warm to room temperature. *n*BuLi in hexane (3.50 mL of a 1.68 M solution in hexane, 5.83 mmol) and TMEDA (0.87 mL, 5.83 mmol) were added dropwise over 30 min to the mixture, and the resulting dark red solution was heated at 60 °C for 3 h. The mixture was cooled to −78 °C and diluted with THF (10 mL). Se (1.20 g, 15.6 mmol) was added in one portion, and the mixture was stirred overnight at room temperature under an argon atmosphere. The mixture was added to H_2O (20 mL), and the two layers were separated. The organic layer was washed with brine (20 mL), dried over $MgSO_4$, filtered, concentrated under reduced pressure, and purified by column chromatography (hexane) to give the title compound (0.09 g, 14%) as dark purple solid: R_f 0.68 (hexane); mp 121–122 °C; ν_{max}(solid state, ATR)/cm^{-1} 1575, 1557, 1440, 1397, 1360, 1285; δ_H (400 MHz, $CDCl_3$) 7.42–7.50 (2 H, m, Ar*H*), 7.51–7.55 (2 H, m, Ar*H*), 7.60 (1 H, s, Ar*H*), 7.61–7.65 (1 H, m, ArH), 8.28 (1 H, d, *J* = 7.7 Hz, Ar*H*), 8.46–8.51 (1 H, m, Ar*H*); δ_C (101 MHz, $CDCl_3$) 119.5 (CH), 120.9 (CH), 123.0 (CH), 125.8 (CH), 127.2 (CH), 127.9 (C), 128.0 (C), 128.2 (C), 133.4 (C), 134.7 (C), 135.7 (C), 138.8 (C), 140.3 (C); *m*/*z* (ES^+) 333.8961 (M^+, $C_{14}H_8{}^{78}Se^{80}Se$ requires 333.8964), 336 (100), 332 (53), 333 (40), 334 (96), 335 (22), 337 (23), 338 (34).

■ ASSOCIATED CONTENT

Ⓢ Supporting Information

UV/vis spectroscopy, X-ray crystallography including structures **6d**, **11d**, and **12b**; additional geometric data for crystal structures **7a,b**, **8**, and **9**; electrochemistry; NMR spectroscopy.This material is available free of charge via the Internet at http://pubs.acs.org.

■ AUTHOR INFORMATION

Corresponding Authors

*E-mail: s.l.horswell@bham.ac.uk.

*E-mail: r.s.grainger@bham.ac.uk.

Notes

The authors declare no competing financial interest.

■ ACKNOWLEDGMENTS

We thank the EPSRC and University of Birmingham for funding. The NMR spectrometers used in this research were obtained through Birmingham Science City: Innovative Uses for Advanced Materials in the Modern World (West Midlands Centre for Advanced Materials Project 2), with support from Advantage West Midlands (AWM) and part funded by the European Regional Development Fund (ERDF).

■ REFERENCES

(1) For reviews on hydrogenases, see: (a) Fontecill-Camps, J. C.; Volbeda, A.; Cavazza, C.; Nicolet, Y. *Chem. Rev.* **2007**, *107*, 4273–4303. (b) Vincent, K. A.; Parkin, A.; Armstrong, F. A. *Chem. Rev.* **2007**, *107*, 4366–4413. (c) Lubitz, W.; Ogata, H.; Rüdiger, O.; Reijerse, E. *Chem. Rev.* **2014**, *114*, 4081–4148.

(2) For structural determination of [FeFe]-hydrogenase, see: (a) Peters, J. W.; Lanzilotta, W. N.; Lemon, B. J.; Seefeldt, L. C. *Science* **1998**, *282*, 1853–1858. (b) Nicolet, Y.; Piras, C.; Legrand, P.; Hatchikian, C. E.; Fontecilla-Camps, J. C. *Structure* **1999**, *7*, 13–23.

(3) For reviews of mimics of [FeFe] hydrogenase, see: (a) Tard, C.; Pickett, C. J. *Chem. Rev.* **2009**, *109*, 2245–2274. (b) Gloaguen, F.; Rauchfuss, T. B. *Chem. Soc. Rev.* **2009**, *38*, 100–108. (c) Capon, J.-F.; Gloaguen, F.; Pétillon, F. Y.; Schollhammer, P.; Talarmin, J. *Coord. Chem. Rev.* **2009**, *253*, 1476–1494. (d) Felton, G. A. N.; Mebi, C. A.; Petro, B. J.; Vannucci, A. K.; Evans, D. H.; Glass, R. S.; Lichtenberger, D. L. *J. Organomet. Chem.* **2009**, *694*, 2681–2699. (e) Tschierlei, S.; Ott, S.; Lomoth, R. *Energy Environ. Sci.* **2011**, *4*, 2340–2352. (f) Wang, N.; Wang, M.; Chen, L.; Sun, L. *Dalton Trans.* **2013**, *42*, 12059–12071. (g) Simmons, T. R.; Berggren, G.; Bacchi, M.; Fontecave, M.; Vincent Artero, V. *Coord. Chem. Rev.* **2014**, *270–271*, 127–150.

(4) Wright, R. J.; Lim, C.; Tilley, T. D. *Chem.—Eur. J.* **2009**, *15*, 8518–8525.

(5) (a) Samuel, A. P. S.; Co, D. T.; Stern, C. L.; Wasielewski, M. R. *J. Am. Chem. Soc.* **2010**, *132*, 8813–8815. (b) Poddutoori, P.; Co, D. T.; Samuel, A. P. S.; Kim, C. H.; Vagnini, M. T.; Wasielewski, M. R. *Energy Environ. Sci.* **2011**, *4*, 2441–2450.

(6) Topf, C.; Monkowius, U.; Knör, G. *Inorg. Chem. Commun.* **2012**, *21*, 147–150.

(7) Mebi, C. A.; Noll, B. C.; Gao, R.; Karr, D. *Z. Anorg. Allg. Chem.* **2010**, *636*, 2550–2554.

(8) (a) For a review, see: Harb, M. K.; Apfel, U.-P.; Sakamoto, T.; El-khateeb, M.; Weigand, W. *Eur. J. Inorg. Chem.* **2011**, 986–993. (b) For the first example of an iron carbonyl cluster bound to selenium, see: Hieber, W.; Gruber, J. *Z. Anorg. Allg. Chem.* **1958**, *296*, 91–103.

(9) Gao, S.; Fan, J.; Sun, S.; Peng, X.; Zhao, X.; Hou, J. *Dalton Trans.* **2008**, 2128−2135.
(10) Apfel, U.-P.; Halpin, Y.; Gottschldt, M.; Görls, H.; Vos, J. G.; Weigand, W. *Eur. J. Inorg. Chem.* **2008**, 5112−5118.
(11) Song, L.-C.; Gai, B.; Wang, H.-T.; Hu, Q.-M. *J. Inorg. Biochem.* **2009**, *103*, 805−812.
(12) Harb, M. K.; Niksch, T.; Windhager, J.; Görls, H.; Holze, R.; Lockett, L. T.; Okumura, N.; Evans, D. H.; Glass, R. S.; Lichtenberger, D. L.; El-khateeb, M.; Weigand, W. *Organometallics* **2009**, *28*, 1039−1048.
(13) Harb, M. K.; Apfel, U.-P.; Kübel, J.; Görls, H.; Felton, G. A. N.; Sakamoto, T.; Evans, D. H.; Glass, R. S.; Lichtenberger, D. L.; El-khateeb, M.; Weigand, W. *Organometallics* **2009**, *28*, 6666−6675.
(14) Harb, M. K.; Windhager, J.; Daraosheh, A.; Görls, H.; Lockett, L. T.; Okumura, N.; Evans, D. H.; Glass, R. L.; Lichtenberger, D. L.; El-khateeb, M.; Weigand, W. *Eur. J. Inorg. Chem.* **2009**, 3414−3420.
(15) Harb, M. K.; Görls, H.; Sakamoto, T.; Felton, G. A. N.; Evans, D. H.; Glass, R. S.; Lichtenberger, D. L.; El-Khateeb, M.; Weigand, W. *Eur. J. Inorg. Chem.* **2010**, 3976−3985.
(16) Gao, W.; Song, L.-C.; Yin, B.-S.; Zan, H.-N.; Wang, D.-F.; Song, H.-B. *Organometallics* **2011**, *30*, 4097−4107.
(17) Harb, M. K.; Windhager, J.; Niksch, T.; Görls, H.; Sakamoto, T.; Smith, E. R.; Glass, R. S.; Lichtenberger, D. L.; Evans, D. H.; El-khateeb, M.; Weigand, W. *Tetrahedron* **2012**, *68*, 10592−10599.
(18) Song, L.-C.; Li, Q.-L.; Feng, Z.-H.; Sun, X.-J.; Xie, Z.-J.; Song, H.-B. *Dalton Trans.* **2013**, *42*, 1612−1626.
(19) Song, L.-C.; Gai, B.; Feng, Z.-H.; Du, Z.-Q.; Xie, Z.-J.; Sun, X.-J.; Song, H.-B. *Organometallics* **2013**, *32*, 3673−3684.
(20) Trautwein, R.; Almazahreh, L. R.; Görls, H.; Weigand, W. *Z. Anorg. Allg. Chem.* **2013**, *639*, 1512−1519.
(21) Grainger, R. S.; Procopio, A.; Steed, J. W. *Org. Lett.* **2001**, *3*, 3565−3568.
(22) Grainger, R. S.; Patel, B.; Kariuki, B. M. *Angew. Chem., Int. Ed.* **2009**, *48*, 4832−4835.
(23) Grainger, R. S.; Patel, B.; Kariuki, B. M.; Male, L.; Spencer, N. *J. Am. Chem. Soc.* **2011**, *133*, 5843−5852.
(24) Patel, B.; Carlisle, J.; Bottle, S. E.; Hanson, G. R.; Kariuki, B. M.; Male, L.; McMurtrie, J. C.; Spencer, N.; Grainger, R. S. *Org. Biomol. Chem.* **2011**, *9*, 2336−2344.
(25) Allenmark, S.; Grainger, R. S.; Olsson, S.; Patel, B. *Eur. J. Org. Chem.* **2011**, 4089−4092.
(26) For reviews on the synthesis and application, including metal coordination chemistry, of 1,8-*peri*-substituted naphthalene dichalcogenides and related systems, see: (a) Kilian, P.; Knight, F. R.; Woollins, J. D. *Coord. Chem. Rev.* **2011**, *255*, 1387−1413. (b) Kilian, P.; Knight, F. R.; Woollins, J. D. *Chem.—Eur. J.* **2011**, *17*, 2302−2328. For the first report of an $Fe_2(CO)_6$ complex containing a naphthalene 1,8-dithiolate ligand, see: (c) Teo, B.-K.; Wudl, F.; Hauser, L. J.; Kruger, A. *J. Am. Chem. Soc.* **1977**, *99*, 4862−4863.
(27) Meinwald, J.; Dauplaise, D.; Wudl, F.; Hauser, J. J. *J. Am. Chem. Soc.* **1977**, *99*, 255−257.
(28) Fuller, A. L.; Knight, F. R.; Slawin, A. M.; Woollins, J. D. *Eur. J. Inorg. Chem.* **2010**, *25*, 4034−4043.
(29) Press, D. J.; Back, T. G. *Org. Lett.* **2011**, *13*, 4104−4107.
(30) Meinwald, J.; Dauplaise, D.; Clardy, J. *J. Am. Chem. Soc.* **1977**, *99*, 7743−7744.
(31) Block, E.; Eswarakrishnan, V.; Gernon, M.; Ofori-Okai, G.; Saha, C.; Tang, K.; Zubieta, J. *J. Am. Chem. Soc.* **1989**, *111*, 658−665.
(32) Manna, D.; Mugesh, G. *J. Am. Chem. Soc.* **2012**, *134*, 4269−4279.
(33) Ashe, A. J.; Kampf, J. W.; Savla, P. M. *Heteroatom Chem.* **1994**, *5*, 113−119.
(34) Works, C. F. *J. Chem. Educ.* **2007**, *84*, 836−838.
(35) Mebi, C. A.; Felton, M. C. *J. Ind. Chem. Res.* **2011**, *10*, 166−170.
(36) Tesmer, M.; Vahrenkamp, H. *Eur. J. Inorg. Chem.* **2001**, 1183−1188.
(37) Zanello, P. *Inorganic Electrochemistry; Theory, Practice and Application*; The Royal Society of Chemistry: Cambridge, 2003.
(38) Izutsu, K. *Acid-Base Dissociation Constants in Dipolar Aprotic Solvents*; Blackwell Scientific Publications: Oxford, 1990.
(39) Bhugun, I.; Lexa, D.; Savéant, J. *J. Am. Chem. Soc.* **1996**, *118*, 3982−3983.
(40) Andrieux, C. P.; Blocman, C.; Dumas-Bouchiat, J.; M'Halla, F.; Savéant, J. *J. Electroanal. Chem.* **1980**, *113*, 19−40.
(41) Savéant, J.; Su, K. B. *J. Electroanal. Chem.* **1984**, *171*, 341−349.
(42) Gloaguen, F.; Lawrence, J. D.; Rauchfuss, T. B.; Bernard, M.; Rohmer, M. *Inorg. Chem.* **2002**, *41*, 6573−6582.
(43) Felton, G. A. N.; Glass, R. S.; Lichtenberger, D. L.; Evans, D. H. *Inorg. Chem.* **2006**, *45*, 9181−9184.
(44) (a) Borg, S. J.; Behrsing, T.; Best, S. P.; Razavet, M.; Liu, X.; Pickett, C. J. *J. Am. Chem. Soc.* **2004**, *126*, 16988−16999. (b) Borg, S. J.; Ibrahim, S. K.; Pickett, C. J.; Best, S. P. *C. R. Chimie* **2008**, *11*, 852−860.
(45) Armarego, W. L.; Perrin, D. D. *Purification of Laboratory Chemicals*, 4th ed.; Butterworth-Heinemann: Oxford, 1998.
(46) Fulmer, G. R.; Miller, A. J. M.; Sherden, N. H.; Gottlieb, H. E.; Nudelman, A. N.; Stoltz, B. M.; Bercaw, J. E.; Goldberg, K. I. *Organometallics* **2010**, *29*, 2176−2179.
(47) Coles, S. J.; Gale, P. A. *Chem. Sci.* **2012**, *3*, 683−689.
(48) *CrysAlisPro*, Agilent Technologies, 2014.
(49) *CrystalClear-SM Expert*, Rigaku, 2012.
(50) Sheldrick, G. M. *Acta Crystallogr.* **2008**, *A64*, 112−122.
(51) Dolomanov, O. V.; Bourhis, L. J.; Gildea, R. J.; Howard, J. A. K.; Puschmann, H. *J. Appl. Crystallogr.* **2009**, *42*, 339−341.